Structural insights into SUMO E1-E2 interactions in Arabidopsis uncovers a distinctive platform for securing SUMO conjugation specificity across evolution

Bing Liu[1], L. Maria Lois[2] and David Reverter[1*]

[1]Institut de Biotecnologia i de Biomedicina. Departament de Bioquimica i Biologia Molecular. Serra Hunter Fellow. Universitat Autonoma de Barcelona, 08193 Barcelona, Bellaterra, Spain.

[2]Center for Research in Agricultural Genomics-CRAG. Edifici CRAG-Campus UAB, Bellaterra 08193 Barcelona, Spain.

*To whom the correspondence should be addressed: David Reverter, Universitat Autonòma de Barcelona, 08193 Bellaterra, Barcelona, Spain, Ph: +34 93 5868955, FAX: (93)5812011, E-mail: david.reverter@uab.cat

Abstract

SUMOylation of proteins involves the concerted action of the E1-activating enzyme, E2-conjugating enzyme and E3-ligases. An essential discrimination step in the SUMOylation pathway corresponds to the initial interaction between E1 ubiquitin-fold domain (UFD) and E2 enzymes. Although E2 orthologs possess high sequence identity, the E2 binding region of the UFD domains have diverged across evolution. Moreover, in reciprocal in vitro conjugation reactions Arabidopsis E1 and E2 SCE1 fail to interact efficiently with cognate human E2 Ubc9 and E1 partners, respectively. To gain more insights into the properties of this interface in evolutionary distant organisms, we solved the crystal structure of SUMO E2 SCE1 and its complex with E1 UFD in Arabidopsis. In addition to a few common structural determinants, the interface between the E1 UFD and E2 in Arabidopsis is distinct compared with human and yeast, in particular by the presence of a longer α-helix in the Arabidopsis UFD domain. Despite the variability of E1 UFD domains in these surfaces, they establish specific interactions with highly conserved surfaces of their cognate E2 enzymes. Functional analysis of the different E2 interface residues between human and Arabidopsis revealed Val37 (Met36 in human), as a determinant that provides specificity in the E1-E2 recognition in plants.

1. Introduction

Small ubiquitin-related modifier (SUMO) protein is one of the most extensively studied ubiquitin-like proteins (Ubls) present in eukaryotes. Yeast and invertebrates have a single SUMO protein named Smt3, while vertebrates have several SUMO proteins. Mammalians such as human express four SUMO proteins. SUMO2 and SUMO3 share 97% sequence identity and cannot be distinguished by antibodies [1,2]. However, SUMO1 is quite different from SUMO2/3 and only shares ~47% sequence identity with SUMO1 and SUMO2 [2]. In plants, SUMO conjugation machinery displays high complexity according to isoform number and variability [3,4]. Although only few studies have addressed the biological relevance of this molecular complexity [5–7], the diverse biological function of SUMOylation in plant development and plant responses to environmental stresses could benefit from the existence of isoforms dedicated to SUMOylate proteins under specific physiological conditions. Accordingly, increasing evidences suggest that a deep knowledge of plant SUMOylation could provide novel strategies for increasing crop productivity [4,8,9]. The best-characterized plant SUMOylation system belongs to Arabidopsis [6]. In Arabidopsis, there are eight encoding genes of SUMO isoforms (AtSUMO), but only AtSUMO1, AtSUMO2, AtSUMO3, and AtSUMO5 are expressed [10,11]. Among them, AtSUMO1 and AtSUMO2, which share 83% sequence identity, are the highest expressed isoforms and double knock-out mutants *sumo1sumo2* display embryo lethality [9,12–14].

SUMO is conjugated to target proteins through a three-step enzyme cascade as ubiquitin via SUMO E1 activating enzyme, E2 conjugating enzyme, and E3 ligase [1,2]. In the model proposed for the SUMO/Ubl conjugation pathway, the E2 conjugating enzyme interacts with the E1 activating enzyme by means of the UFD domain [15–18]. The structure of the UFD-E2 interaction is known for ubiquitin, Nedd8, and SUMO systems, showing a direct binding of E2 to the E1 UFD domain [17–23]. The UFD domain is located in the C-terminal end and connected to the E1 active adenylation domain through a flexible hinge. During the thioester transfer between E1 and E2, the UFD domain undergoes a rotation to bring the catalytic cysteine residues of E1 and E2 into proximity for thioester transfer [17,18,24–26]. Moreover, crystal structure of ubiquitin E1-E2 complex reveals a direct interaction of E1 and E2 through their catalytic cysteine domains, which occurs after UFD-E2 binding and a significant rotation of the UFD domain, providing structure insights for the E1 E2 thioester transfer [18,24]. This interaction was also proposed in the SUMO pathway by NMR analyses. However, UFD-E2 interactions (Kd= 1.2μM) display much

higher affinity than the catalytic cysteine domain interactions (Kd= 87μM), consistent with a major role of E1 UFD domain as the initial E2 binding platform [27].

Structural and functional data indicate that the UFD-E2 interactions represent the first contacts between the E1-activating enzyme and the E2-conjugating enzyme, providing an important discrimination step for the pathway [28,29]. UFD-E2 interactions have been revealed essential to provide specificity between the different systems of ubiquitin-like modifiers (i.e. SUMO, Nedd8, ubiquitin…). In the SUMO system, this interaction also provides specificity across species, despite the high homology between the E2-conjugating enzymes [30]. The UFD domains show little protein sequence homology across distant species, and it is even lower when considering just the E2 binding region or LHEB2 domain (*Low Homology region involved in E2 Binding 2*) [31]. However, the opposite is found in close related species, in which the LHEB2 domain display higher conservation than the UFD domain highlighting its crucial role [22,31].

Previous structural studies of the SUMO UFD-E2 complex in yeast and human revealed two alternative UFD interaction interfaces [20–22], in which particular contacts with a highly conserved E2 structure take place in each species. Despite the 65% sequence identity between human and Arabidopsis SUMO E2 conjugating enzymes, human Ubc9 cannot complement Arabidopsis SCE1 in our in vitro conjugating assays using RanGAP1 as a model substrate, and vice versa. As a consequence of the amino acid sequence divergence found between Arabidopsis, human and yeast UFD domains, the study of Arabidopsis E1-E2 interactions cannot rely only on predictive models, and a structural analysis is required to reveal the particular contacts between Arabidopsis E1 and E2 enzymes.

In order to elucidate the structural determinants for such exquisite evolutionary specificity in the interface of the UFD-E2 interaction, we have solved the crystal structure of the Arabidopsis E2-conjugating enzyme (AtSCE1), alone at a high resolution (1.2 Å) and in complex with the Arabidopsis UFD domain (AtUFD) of the E1-conjugating enzyme at 1.8 Å resolution. We have compared the Arabidopsis UFD-E2 domain complex interface with the human and yeast systems and performed biochemical and mutagenesis analysis to understand the role of the interface in the specificity of the SUMO conjugation pathway. Our results indicate that Arabidopsis UFD provides a novel molecular strategy for E2 selection, not interchangeable with its human and yeast orthologs.

2. Materials and methods

2.1 Cloning, protein expression and purification

Expression constructs were generated by a standard PCR-based cloning method. Arabidopsis E1 heterodimers, SUMO1 and 2, SCE1, UFD and UFDC domain, as well as human E1 heterodimers, SUMO1 and 2, Ubc9, were cloned to pET28a tagged with 6×His at the N-terminal. Point mutations were created using the QuickChange site-directed mutagenesis kit (Stratagene). *Escherichia coli* BL21(DE3) plysS containing the expression vector were grown in Luria Bertani medium with chloramphenicol (17 μg/mL) and kanamycine (50 μg/mL) at 37 °C until the OD600 reached to 0.8. Expression was induced by 0.1mM IPTG, followed by overnight culturing at 28 °C. Recombinant proteins were purified by nickel-nitrilotriacetic acid agarose resin (Qiagen) and dialyzed against 250 mM NaCl, 20 mM Tris-HCl (pH 8.0), 1 mM β-mercaptoethanol in the presence of thrombin protease overnight at 4 °C to remove the 6×His tag. Proteins were further purified by gel filtration chromatography on a Superdex75 column (GE Healthcare), which was equilibrated in 250mM NaCl, 20mM Tris-HCl pH 7.5, 1mM β-mercaptoethanol.

2.2. Protein complex preparation and crystallization

AtSCE1 and UFD or UFDC complexes were made by mixing equimolar amounts of proteins and purified by gel filtration chromatography using a Superdex75 column. AtSCE1 and UFD or UFDC were co-eluted in a single peak in buffer containing 100 mM NaCl, HEPES pH 7.0, 1 mM β-mercaptoethanol, and confirmed by SDS-PAGE. Purified protein complex was concentrated to 15 g/L using an Amicon Ultra-10K ultrafiltration device (Millipore) prior to crystallization. Crystals were grown at 18 °C by the sitting-drop vapor diffusion method by mixing the protein with an equal volume of reservoir solution containing 0.1 M Bis-tris pH 5.5, 25% w/v PEG3350 for AtSCE1, or containing 15% PEG6000, 5% glycerol for UFDC-AtSCE1 complex. AtSCE1 crystals appeared after one week, while UFDC-AtSCE1 crystals appeared after several months. Big crystals were soaked in mother liquor supplemented with gradually increasing concentration of 5%, 10%, 20% (v/v) glycerol and flash frozen in liquid nitrogen.

2.3. Data collection, structure determination and refinement

Diffraction data were collected to 1.20 Å resolution for AtSCE1 and 1.8 Å for UFDC-AtSCE1 complex at ALBA synchrotron in Barcelona (BL13-XALOC beamline) [32]. Data were processed with XDS [33] and scaled, reduced, and further analyzed

using CCP4 [34]. More details are shown in Table 1. The structure of AtSCE1 was determined by molecular replacement method using the full length human Ubc9 (PDB code 1U9B) as a search model in PHASER [35]. The structure of UFDC-AtSCE1 complex was determined by molecular replacement method using the solved AtSCE1 as a search model in PHASER [35]. Initial electron density was manually improved to build up the final model using Coot [36], and the refinement was performed using Phenix [37]. Refinement statistics are shown in Table1.

2.3. In vitro conjugation reaction and pull-down assays

SUMO swapping conjugation assays were performed in reactions containing 20 mM Bis-tris propane pH 8.5, 5 mM $MgCl_2$, 0.1% Tween 20, 50 mM NaCl, 1m M DTT, 1 mM ATP, 150 nM E1 heterodimer, 300 nM E2, 10 μM RanGAP1, and 10 μM SUMO protein. SUMO conjugation assays with mutants of the *Arabidopsis* SCE1 were performed in reactions containing the same buffer but with Bis-tris propane pH 7.5 instead. Reactions were incubated at 37 °C and aliquots were mixed with loading buffer for analysis by SDS-PAGE, followed by staining with coomassie brilliant blue.

Ni^{2+} Sepharose 6 Fast Flow beads (GE healthcare) were washed with assay buffer containing 100 mM NaCl, 20 mM Bis-tris propane pH 7.5, 0.1% Tween 20, 1 mM DTT and incubated with 30 μg His-AtUFDC for 1 hour. The beads were then incubated with the same buffer containing 2% BSA for 1 hour to block the unspecific binding, followed by washing three times with the assay buffer. 10 μg of the untagged E2 was mixed in 300 μl of assay buffer and added in the beads, followed by incubation for 1 hour. The beads were then washed three times and elute with assay buffer containing 500 mM imidazole. Elution aliquots were mixed with loading buffer and analyzed by SDS-PAGE with coomassie brilliant blue staining.

2.4. Temperature and urea induced unfolding assays

The tryptophan fluorescence spectra of temperature induced unfolding measurements were taken at excitation wavelength 280 nM and emission 340 nM in PBS buffer containing 0.15 g/L proteins. Data collection was at temperature from 25 °C to 80 °C with 1 °C steps and 1 minute between steps for equilibration in triplicates. Fraction unfolded was obtained by plotting the normalized fluorescence versus the corresponding temperatures. The urea induced unfolding were performed in PBS buffer by mixing 0.15 g/L proteins with increasing concentrations of urea (0 – 9M) at 25 °C overnight to reach equilibrium. Tryptophan emission spectra of urea

induced unfolding were obtained by setting the excitation wavelength at 280 nM and collecting emission in the 300-400 nM range These spectra were quantified as the center of spectral mass (v) according to equation $v = \Sigma v_i F_i / \Sigma F_i$ where F_i stands for the fluorescence emission at a given wavelength (v_i) and the summation is carried out over the range of appreciable values of F [38,39]. Fraction unfolded was obtained by plotting the normalized center of spectral mass versus the corresponding urea concentrations. All measurements were conducted using Jasco FP-8200 spectrofluorimeter. Curves were generated using GraphPad Prism 7.0.

3. Results and discussion

3.1. E1 and E2 enzymes are specific between human and Arabidopsis

An intriguing question in the field deals with the lack of compatibility between enzymes of the SUMO conjugation pathway from different species, even though the high sequence identity present between E2 enzymes orthologs. We have conducted in vitro SUMO conjugation reactions swapping the SUMOylation components of Arabidopsis and human, including SUMO proteins, E1, and E2. Human RanGAP1, which contains the SUMO consensus motif Ψ-K-X-D/E [28,40], can be sufficiently conjugated by the SUMO machinery from both species, validating it as an in vitro universal SUMO substrate in E3-independent SUMO conjugation assays [41]. In conjugation assays containing human or Arabidopsis E1 and E2, the purified human RanGAP1 is quantitatively SUMOylated and migrates at ~32kD, consistent with the molecular weight of single SUMO modification (**Fig. 1A,B**).

The results of SUMO swapping between human and Arabidopsis show differences in conjugation rate and SUMO ortholog specificity. Under our experimental conditions, the human E1 and E2 facilitate SUMO conjugation to RanGAP1 more efficiently than the Arabidopsis E1 and E2 pair. This higher efficiency is observed independently on the SUMO1 ortholog (hSUMO1, hSUMO2, AtSUMO1 or AtSUMO2) present in the assay. The Arabidopsis E1 and E2 pair catalyze the conjugation of AtSUMO1 and AtSUMO2 to RanGAP1 to a similar extend, consistently with results obtained using the plant substrate AtCAT3 [13], although with lower efficiency than the human E1 and E2. This reduced activity of the Arabidopsis E1 and E2 is more dramatic when the human SUMO1 or SUMO2 are included in the assay. (**Fig. 1A,B**). These results are consistent with a described role of Arabidopsis E1 in SUMO isoform selection [13], which has not been reported for human E1 up to date. The present results suggest the existence of molecular determinants in Arabidopsis E1 that contribute to confer higher selectivity in SUMO recognition than the human E1 ortholog. Future structural analysis will be required to uncover these molecular determinants present in the Arabidopsis system, which we speculate could be the result of the higher divergence between SUMO isoforms present in plants. Nonetheless, these results show that SUMOs can be interchanged between systems at different levels, indicating that probably the observed complete incompatibility between species raises from the E2 interaction to E1 and/or to the SUMO-thioester transfer between E1 and E2 (**Fig. 1C**).

E2-conjugating enzymes display a 65% sequence identity between human and Arabidopsis. When similar SUMO conjugation reactions were performed combining

human and Arabidopsis E1 and E2 enzymes, SUMOylated RanGAP1 could not be detected in trace amounts in the Arabidopsis E1 and human E2 combination after 120 min reaction (**Fig. 1D**). These results indicate despite that the formation of the E1-SUMO thioester could be achieved by combining human or plant SUMOs **(Fig. 1A,C)**, the whole SUMO conjugation process relies on compatible interactions between E1 and E2 enzymes, which are necessary for the SUMO-thioester transfer from the E1 to the E2-conjugating enzyme. This organism-dependent specificity between human and Arabidopsis E1 and E2 interaction is consistent with results obtained between human and *P. falciparum* systems [21,30].

3.2. Complex formation and crystallization

To further define the E1-E2 interaction interface between human and Arabidopsis by protein crystallography, we have purified the recombinant Arabidopsis E2-conjugating enzyme (AtSCE1) and the E1 UFD domain. AtSCE1 was expressed as a full-length protein (Met1 to Val160) in a pET28 vector, which includes a N-terminal His-tag extension to facilitate its purification. The UFD domain of the Arabidopsis E1-activating enzyme was expressed in two different versions: a short version including only the UFD domain (Ubiquitin-like Fold Domain) from Ser436 to Thr549 (AtUFD); and a longer version including the C-terminal extension, from Ser436 to Glu625 (AtUFDC). AtUFD and AtUFDC, were cloned in a pET28 vector, which includes a N-terminal His-tag for affinity purification. Recombinant expression in *E. coli* of both proteins was successful and high protein amounts could be retrieved after the final purification step.

Complex formation between AtSCE1 and AtUFDC or AtUFD was conducted by mixing equimolar amounts of both components and running a size-exclusion chromatography (**Fig. 2A,B**). The fractions of the complex were pooled and concentrated to set up crystallization screens. Interestingly, only the complex including the C-terminal extension of the UFD domain (AtUFDC) produced good diffraction quality crystals after several months at 18°C. The role of this C-terminal extension of the SAE2 E1 large subunit has not been completely clarified, although it might contribute to subcellular compartment localization both in human and Arabidopsis, as it contains a nuclear localization signal [7,42], but it does not seem relevant for the catalytic activity despite the presence of a SIM (SUMO interaction motif) observed in the active form of the SUMO E1 crystal structure [15,43].

3.3. Structure of Arabidopsis *E2 alone and in complex with the E1 UFD domain*

The structure of the Arabidopsis E2-conjugating enzyme, AtSCE1, was solved at 1.2 Å resolution (**Fig. 3A)** (**Table 1**), which allows the visualization of structural details in the final electron density maps, such as the presence of residues with alternate conformations. Intriguingly, the final electron density reveals a double conformation of a 6 residues helical stretch in the C-terminal region of AtSCE1, between Tyr135 and Asp141. Despite this particular feature, the Arabidopsis AtSCE1 structure is highly similar to the structure of human Ubc9 (65% identity and rmsd=0.88 Å for 155 aligned residues) (**Fig. 3D**). The major differences in the backbone trace with human Ubc9 (PDB code 1A3S) [44] corresponds to the β1-β2 loop, and to a small loop at the end of the β4 strand, produced by a 3 residue substitution (P-Q-G in *A.thaliana,* E-P-P in human) (**Fig. 3D**).

We have also solved the crystal structure of AtSCE1 in complex with the UFDC domain of the Arabidopsis E1-activating enzyme at 1,8 Å resolution (**Fig. 3C**) (**Table 1**), however the UFDC C-terminal extension was not observed in the final electron density maps. The structure of the complex was solved by molecular replacement using our previous AtSCE1 structure as a search model. As detailed later, the interface region in the AtSCE1 E2-conjugating enzyme comprises contacts in the α1 helix and in the β1-β2 loop with the β-grasp fold of the E1 UFD domain (**Fig. 3C**), as expected from previous structures of the complex in human and yeast [20–22]. The structure of AtSCE1 in the complex is nearly identical to its isolated form (rmsd=0.35 Å for 155 aligned residues), with the most notable difference being the slight variation in the β1-β2 loop conformation (**Fig. 3B**). Compared with a prior complex structure in human (5FQ2), AtSCE1 displays high degree of similarity with Ubc9 (rmsd=0.47 Å for 155 aligned residues), with a slight shift in the β1-β2 loop to accommodate the AtUFD surface, but superimposition of the E2 moieties results in a shift in the orientation of their cognate UFD domains (**Fig. 3E)**. Moreover, alignment of the UFD domains between human and Arabidopsis (30% identity and rmsd=1.30 Å for 93 aligned residues) also displays a notable rotation of SCE1 and Ubc9 across the β-grasp fold (**Fig. 3F)**. Similar shifted orientations between the two moieties in the complex are also observed when compared with the yeast UFD-Ubc9 complex (**Figs. 3G, H, I).**

3.4. Structural analysis of the interface between Arabidopsis *E1 and E2.*

The binding surface in AtSCE1 resembles the structures of the complex in human and yeast, and it is formed by contacts between the α1 helix and the β1-β2

loop of AtSCE1. Major specific contacts include Val37, Leu39 and Met40 from the β1-β2 loop and Arg7, Arg14, Lys15, Arg18 and Lys19 from the α1 helix basic patch (**Fig. 4A)**. Differences between human and Arabidopsis in the E2 contact residues are few, only the presence of Arg7 (leucine in human), Lys28 (valine in human) and Val37 (Met36 in human) (**Fig. 4B)**. Moreover, Glu67, which is not located in the SCE1 α1-helix/β1-β2 binding module, forms a new hydrogen bond not present in human (**Fig. 4)**. Previous mutational analysis of human Ubc9 contact residues, such as the basic patch in α1 helix, revealed its major role for the interaction to the UFD E1 domain, and was proven to be essential for the transfer of SUMO between E1 and E2 enzymes in the conjugation reaction [45]. Interestingly, despite their high conservation between human and Arabidopsis, E2-conjugating enzymes are not interchangeable in our in vitro conjugation assays (**Fig. 1D)**.

The structure of the AtUFD domain of Arabidopsis E1-activating enzyme displays a similar fold as the human or yeast counterparts (20% identity and rmsd=2.17 Å for 91 aligned residues between Arabidopsis and yeast UFD). However, a major structural difference in AtUFD corresponds to the presence of a longer α2-helix (**Fig. 5A),** resulting from a sequence insertion occurring in Arabidopsis (**Fig. 5C)**. Residues from this novel longer α2 helix together with residues emanating from central β-sheet of the AtUFD (β4-β2-β3) directly participate in the interface with the E2 enzyme (**Fig. 5B)**. We have previously defined the interacting region between E2 and UFD E1 domain as *Low Homology region involved in E2 Binding 2* (LHEB2) [31], because it displays a lower homology in comparison to the rest of the UFD domain: i.e. UFD sequence identity between human and Arabidopsis is 31%, but is reduced to 11% when considering only the LHEB2 binding region. The LHEB2 can be divided in two regions, each establishing interactions with either the α1 helix or the β1-β2 loop of AtSCE1. Interestingly, a unique contact, not present in human or yeast, is observed in Arabidopsis between AtUFD Asn474 and AtSCE1 Glu67, a region far from the α1-helix/β1-β2 loop module of the E2-conjugating enzyme (**Fig. 5B)**.

The first contact region in the AtUFD domain is composed by Glu479, Asp483 and Glu516, which contact the positive charged groups of the AtSCE1 α1-helix (Arg14, Lys15, Arg18 and Lys19) and by Leu469 and Leu518, which are buried in a hydrophobic patch formed by the aliphatic side chain atoms of the aforementioned AtSCE1 α1 helix basic residues (**Fig. 5B)**. Interestingly, Phe522 occupies this region in human, whereas in yeast it is occupied by Tyr489 (**Fig. 5C,D)**, all of them buried in a similar aliphatic pocket wedged between basic residues of the AtSCE1 α1 helix [22]. Other contacts present in the AtSCE1 α1 helix include the unique Arg7 (leucine in

human), and Ala11, which interact with AtUFD Met471 (glutamine or leucine in human and yeast, respectively) (**Fig. 5B,D)**.

The second region of AtUFD E1 domain includes contacts with the β1-β2 loop surface of AtSCE1, and is composed by interactions from the β2-β3 loop and the longer α2 helix of AtUFD. Leu476, Asp485, Asn491, Tyr492 and Pro504 side chains are the major contacts within the AtUFD domain (**Fig. 5B,C)**. In human and yeast this region is formed by a different type of contacts (**Fig. 5C,D)**, only few similar to Arabidopsis: the central Leu476 (isoleucine and leucine in human and yeast, respectively) and the backbone hydrogen bond contacts between Asn474 and Leu476, with AtSCE1 Val37 and Leu39 (**Fig. 5D)**.

The analysis of the E1 UFD-E2 interfaces between Arabidopsis and human suggest that all contact residue substitutions in the UFD domain across species are accompanied by the compensatory residue substitutions to interact with the E2 enzyme, suggesting a convergent co-evolution of the UFD domains to interact with the conserved residues of the E2 surface. Finally, the structural analysis of our UFD-E2 complex in Arabidopsis in the present work confirms the impaired E2 binding interaction of two predicted AtUFD mutants (L476A, D485A) published previously [31].

3.5. SUMO conjugation assays with mutants of the Arabidopsis *SCE1*

Since SUMO modifier swapping was not a major issue for in vitro conjugation assays between human and Arabidopsis, we attribute the specificity of the SUMO conjugation reaction to the E1-E2 interaction (**Fig. 1)**. This interaction has been proposed to be an essential recognition step for the recruitment of E2 on the E1-conjugation enzyme surface. Our structural analysis indicates that the E2 surface in contact with the UFD domain is highly conserved between Arabidopsis and human (**Fig. 4A,B)**, with only few modifications: Arg7-Gly8 (Leu-Ser in human); Lys28 (Val in human), and Val37 (Met in human) (**Fig. 4A,B)**. To investigate the structural determinants for the specificity between Arabidopsis and human E2 enzymes, we have produced 5 different mutants in Arabidopsis AtSCE1 interface with the UFD domain: R7L; R7L/G8S; R7L/G8S/K28V; R7L/G8S/K28V/V37M; V37M. All residues in AtSCE1 have been replaced by the corresponding residues in human Ubc9 (**Fig. 4B).** Additionally, we have also assessed the role of the distinctive contact in Arabidopsis outside the α1-helix/β1-β2 loop module, by producing the AtSCE1 E67S point mutant.

In vitro conjugation assays were conducted using the Arabidopsis enzymes with RanGAP1 as a model substrate. Replacement of AtSCE1 Arg7 and Gly8 (by Leu and

Ser in human, respectively), present at the beginning of the α1-helix, did not show any defect on the SUMO conjugation and displayed similar activities as the wild-type form (**Fig. 6A)**. Regarding to AtSCE1 Lys28 (Val in human) and Val37 (Met in human), both present in the β1-β2 loop region, only Val37 had a strong effect on the conjugation activity (**Fig. 6A)**. Such loss of the activity is probably caused by an E1 binding defect, since the R7L/G8S/K28V/V37M and V37M mutants also showed a reduced UFD binding in pull-down assays (**Fig. 6B)**. Finally, disruption of the unique contact described in *A.thaliana,* Glu67, only displayed a slight reduction in the conjugation activity (**Fig. 6A,B)**.

To further assess the relevance of the Val37 point mutant, protein stability assays were conducted with AtSCE1 wild type and the R7L/G8S/K28V/V37M tetra-point mutant. Temperature-induced protein unfolding assays, indicate a similar thermal stability for the wild type AtSCE1 (Tm 48.4 °C) and R7L/G8S/K28V/V37M mutant (Tm 49.1 °C) (**Fig. 6C)**. Also, urea-induced protein unfolding assays with wild type and R7L/G8S/K28V/V37M mutant displayed similar half transition concentration values of 2.6 M and 2.4 M urea, respectively (**Fig. 6C)**. These results support the correct structural integrity for the AtSCE1 R7L/G8S/K28V/V37M mutant, probably attributing the SUMO conjugation impairment to a defect in the binding between UFD E1 and E2 enzymes caused by the Val37 substitution for methionine, as confirmed by the correct activity of the AtSCE1 R7L/G8S/K28V triple-mutant (**Fig. 6A)**.

It is worth mentioning here that the Arabidopsis AtSCE1 R7L/G8S/K28V/V37M tetra-mutant, in which most of the contacts with the UFD domain have been replaced for those in human Ubc9, do not display any SUMO conjugation when used as an E2 with human SUMO1 or -2, human E1 and RanGAP1 (data not shown). These results indicate that the different specificities in SUMO conjugation between human and Arabidopsis not only rely on the highly conserved E1 UFD contact surface. Thus, despite the strong conservation between human and Arabidopsis E2 enzymes, surface residues outside the UFD interface in the E2 enzyme are also critical for SUMO specificity across species. Probably these residues outside the UFD interface are required for the interaction with other regions of the E1 enzyme, such as the E1 Cys-domain, as observed in the crystal structures of the ubiquitin E1-E2 complexes captured during the ubiquitin trans-thiolation transfer [18,24].

Interestingly, the different angle orientation of the SUMO E2 enzyme in complex with human, yeast and Arabidopsis SUMO UFD E1 domain probably contributes to provide specificity with its cognate E1 enzyme, thus it might elude steric clashes with other regions of the E1 enzyme during the catalytic trans-thiolation reaction. Our

results are also consistent with the SUMO E2 specificity analysis conducted between human and *Plasmodium falciparum* [21,30], in which the SUMO conjugation reaction was only efficient only after the substitution of half of the E2 enzyme sequence between both species.

4. Conclusion

Our study provides the first detailed atomic structures of the Arabidopsis SUMO E2-conjugating enzyme, AtSCE1, alone and in complex with the UFD domain of the Arabidopsis SUMO E1-activating enzyme. This interaction between E1 and E2 enzymes represents the initial step for the recruitment of the E2 enzyme to the SUMO conjugation pathway. The atomic details in the E1-E2 interface provided by our structure sheds light to the specificity displayed in the SUMO conjugation pathway across species, in which at least three different E1 UFD binding platforms, in human, yeast and plants, have evolved to interact with a highly conserved cognate E2 enzyme. Our study suggests that this evolution is based on the interaction between the E2-conjugating enzyme and the E1 UFD domain, in which modifications on the UFD domain surface occur to compensate mutations that affect its interaction with the conserved surface of the E2 enzyme. Also, despite this high similarity in the E2 conjugating enzymes in the E1 binding interface (more than 65% identity between human and Arabidopsis), they cannot be efficiently interchanged in our in vitro conjugation assays, indicating that these substitutions are critical for efficient cognate E1-E2 species-dependent recognition.

Acknowledgements

B.L. acknowledges his scholarship to the Chinese Research Council program from the Chinese government. We acknowledge the help of the scientists at the BL-13 beamline at the ALBA synchrotron.

Declarations of interest

The authors declare no competing financial interests.

Funding information

This work was supported by grants from the “Ministerio de Economia y Competitividad” BFU2015-66417-P (MINECO/FEDER) to DR, and from the “Fundació La Caixa”, (CaixaImpulse CI17-00028) and from “Ministerio de Ciencia” (BIO2017-89874-R) to LML.

Author Contribution statement

BL conducted all protein expression, crystallization and biochemical analysis. BL and DR solved the crystal structures. LML provided the recombinant expression vectors for Arabidopsis proteins. DR and LML conceived the idea for the project. LML, DR and BL wrote and revised the paper.

References

1 Johnson, E. S. (2004) Protein modification by SUMO. Annu. Rev. Biochem., Annual Reviews **73**, 355–382.

2 Flotho, A. and Melchior, F. (2013) Sumoylation: a regulatory protein modification in health and disease. Annu. Rev. Biochem., Annual Reviews **82**, 357–385.

3 Novatchkova, M., Tomanov, K., Hofmann, K., Stuible, H. and Bachmair, A. (2012) Update on sumoylation: defining core components of the plant SUMO conjugation system by phylogenetic comparison. New Phytol., Wiley Online Library **195**, 23–31.

4 Augustine, R. C. and Vierstra, R. D. (2018) SUMOylation: re-wiring the plant nucleus during stress and development. Curr. Opin. Plant Biol., Elsevier **45**, 143–154.

5 Budhiraja, R., Hermkes, R., Müller, S., Schmidt, J., Colby, T., Panigrahi, K., Coupland, G. and Bachmair, A. (2009) Substrates related to chromatin and to RNA-dependent processes are modified by Arabidopsis SUMO isoforms that differ in a conserved residue with influence on desumoylation. Plant Physiol., Am Soc Plant Biol **149**, 1529–1540.

6 Colby, T., Matthäi, A., Boeckelmann, A. and Stuible, H.-P. (2006) SUMO-conjugating and SUMO-deconjugating enzymes from Arabidopsis. Plant Physiol., Am Soc Plant Biol **142**, 318–332.

7 Castaño-Miquel, L., Seguí, J., Manrique, S., Teixeira, I., Carretero-Paulet, L., Atencio, F. and Lois, L. M. (2013) Diversification of SUMO-activating enzyme in Arabidopsis: implications in SUMO conjugation. Mol. Plant, Elsevier **6**, 1646–1660.

8 Rosa, M. T. G. and Abreu, I. A. (2019) Exploring the regulatory levels of SUMOylation to increase crop productivity. Curr. Opin. Plant Biol., Elsevier **49**, 43–51.

9 Benlloch, R. and Lois, L. M. (2018) Sumoylation in plants: mechanistic insights and its role in drought stress. J. Exp. Bot., Oxford University Press UK **69**, 4539–4554.

10 Novatchkova, M., Budhiraja, R., Coupland, G., Eisenhaber, F. and Bachmair, A. (2004) SUMO conjugation in plants. Planta, Springer **220**, 1–8.

11 Hammoudi, V., Vlachakis, G., Schranz, M. E. and van den Burg, H. A. (2016) Whole-genome duplications followed by tandem duplications drive diversification of the protein modifier SUMO in Angiosperms. New Phytol., Wiley Online Library **211**, 172–185.

12 Saracco, S. A., Miller, M. J., Kurepa, J. and Vierstra, R. D. (2007) Genetic analysis of SUMOylation in Arabidopsis: conjugation of SUMO1 and SUMO2 to nuclear proteins is essential. Plant Physiol., Am Soc Plant Biol **145**, 119–134.

13 Castaño-Miquel, L., Seguí, J. and Lois, L. M. (2011) Distinctive properties of Arabidopsis SUMO paralogues support the in vivo predominant role of AtSUMO1/2 isoforms. Biochem. J., Portland Press Limited **436**, 581–590.

14 Tomanov, K., Ziba, I. and Bachmair, A. (2016) SUMO chain formation by plant enzymes. In Plant Proteostasis, pp 97–105, Springer.

15 Lois, L. M. and Lima, C. D. (2005) Structures of the SUMO E1 provide mechanistic insights into SUMO activation and E2 recruitment to E1. EMBO J., EMBO Press **24**, 439–451.

16 Huang, D. T., Paydar, A., Zhuang, M., Waddell, M. B., Holton, J. M. and Schulman, B. A. (2005) Structural basis for recruitment of Ubc12 by an E2 binding domain in NEDD8's E1. Mol. Cell, Elsevier **17**, 341–350.

17 Huang, D. T., Hunt, H. W., Zhuang, M., Ohi, M. D., Holton, J. M. and Schulman, B. A. (2007) Basis for a ubiquitin-like protein thioester switch toggling E1–E2 affinity. Nature, Nature Publishing Group **445**, 394.

18 Olsen, S. K. and Lima, C. D. (2013) Structure of a ubiquitin E1-E2 complex: insights to E1-E2 thioester transfer. Mol. Cell, Elsevier **49**, 884–896.

19 Huang, D. T., Ayrault, O., Hunt, H. W., Taherbhoy, A. M., Duda, D. M., Scott, D. C., Borg, L. A., Neale, G., Murray, P. J. and Roussel, M. F. (2009) E2-RING expansion of the NEDD8 cascade confers specificity to cullin modification. Mol. Cell, Elsevier **33**, 483–495.

20 Wang, J., Taherbhoy, A. M., Hunt, H. W., Seyedin, S. N., Miller, D. W., Miller, D. J., Huang, D. T. and Schulman, B. A. (2010) Crystal structure of UBA2ufd-Ubc9: insights into E1-E2 interactions in sumo pathways. PLoS One, Public Library of Science **5**, e15805.

21 Reiter, K. H., Ramachandran, A., Xia, X., Boucher, L. E., Bosch, J. and Matunis, M. J. (2016) Characterization and structural insights into selective E1-E2 interactions in the human and Plasmodium falciparum SUMO conjugation systems. J. Biol. Chem., ASBMB **291**, 3860–3870.

22 Liu, B., Lois, L. M. and Reverter, D. (2017) Structural analysis and evolution of specificity of the SUMO UFD E1-E2 interactions. Sci. Rep., Nature Publishing Group **7**, 41998.

23 Walden, H., Podgorski, M. S. and Schulman, B. A. (2003) Insights into the ubiquitin transfer cascade from the structure of the activating enzyme for NEDD8. Nature, Nature Publishing Group **422**, 330.

24 Lv, Z., Rickman, K. A., Yuan, L., Williams, K., Selvam, S. P., Woosley, A. N., Howe, P. H., Ogretmen, B., Smogorzewska, A. and Olsen, S. K. (2017) S. pombe Uba1-Ubc15 structure reveals a novel regulatory mechanism of ubiquitin E2 activity. Mol. Cell, Elsevier **65**, 699–714.

25 Wang, J., Lee, B., Cai, S., Fukui, L., Hu, W. and Chen, Y. (2009) Conformational transition associated with E1-E2 interaction in small ubiquitin-like modifications. J. Biol. Chem., ASBMB **284**, 20340–20348.

26 Elgin, E. S., Sökmen, N., Peterson, F. C., Volkman, B. F., Dağ, Ç. and Haas, A. L. (2012) E2-binding surface on Uba3 β-grasp domain undergoes a conformational transition. Proteins Struct. Funct. Bioinforma., Wiley Online Library **80**, 2482–2487.

27 Wang, J., Hu, W., Cai, S., Lee, B., Song, J. and Chen, Y. (2007) The intrinsic affinity between E2 and the Cys domain of E1 in ubiquitin-like modifications. Mol. Cell, Elsevier **27**, 228–237.

28 Cappadocia, L. and Lima, C. D. (2017) Ubiquitin-like protein conjugation: structures, chemistry, and mechanism. Chem. Rev., ACS Publications **118**, 889–918.

29 Pichler, A., Fatouros, C., Lee, H. and Eisenhardt, N. (2017) SUMO conjugation–a mechanistic view. Biomol. Concepts, De Gruyter **8**, 13–36.

30 Reiter, K., Mukhopadhyay, D., Zhang, H., Boucher, L. E., Kumar, N., Bosch, J. and Matunis, M. J. (2013) Identification of biochemically distinct properties of the small

ubiquitin-related modifier (SUMO) conjugation pathway in Plasmodium falciparum. J. Biol. Chem., ASBMB **288**, 27724–27736.

31 Castaño-Miquel, L., Mas, A., Teixeira, I., Seguí, J., Perearnau, A., Thampi, B. N., Schapire, A. L., Rodrigo, N., La Verde, G., Manrique, S., Coca, M. and Lois, L.M. (2017) SUMOylation inhibition mediated by disruption of SUMO E1-E2 interactions confers plant susceptibility to necrotrophic fungal pathogens. Mol. Plant, Elsevier **10**, 709–720.

32 Juanhuix, J., Gil-Ortiz, F., Cuní, G., Colldelram, C., Nicolás, J., Lidón, J., Boter, E., Ruget, C., Ferrer, S. and Benach, J. (2014) Developments in optics and performance at BL13-XALOC, the macromolecular crystallography beamline at the ALBA synchrotron. J. Synchrotron Radiat., International Union of Crystallography **21**, 679–689.

33 Kabsch, W. (2010) Xds. Acta Crystallogr. Sect. D Biol. Crystallogr., International Union of Crystallography **66**, 125–132.

34 Winn, M. D., Ballard, C. C., Cowtan, K. D., Dodson, E. J., Emsley, P., Evans, P. R., Keegan, R. M., Krissinel, E. B., Leslie, A. G. W. and McCoy, A. (2011) Overview of the CCP4 suite and current developments. Acta Crystallogr. Sect. D Biol. Crystallogr., International Union of Crystallography **67**, 235–242.

35 Storoni, L. C., McCoy, A. J. and Read, R. J. (2004) Likelihood-enhanced fast rotation functions. Acta Crystallogr. Sect. D Biol. Crystallogr., International Union of Crystallography **60**, 432–438.

36 Emsley, P. and Cowtan, K. (2004) Coot: model-building tools for molecular graphics. Acta Crystallogr. Sect. D Biol. Crystallogr., International Union of Crystallography **60**, 2126–2132.

37 Adams, P. D., Afonine, P. V, Bunkóczi, G., Chen, V. B., Davis, I. W., Echols, N., Headd, J. J., Hung, L.-W., Kapral, G. J. and Grosse-Kunstleve, R. W. (2010) PHENIX: a comprehensive Python-based system for macromolecular structure solution. Acta Crystallogr. Sect. D Biol. Crystallogr., International Union of Crystallography **66**, 213–221.

38 Silva, J. L., Miles, E. W. and Weber, G. (1986) Pressure dissociation and conformational drift of the. beta. dimer of tryptophan synthase. Biochemistry, ACS Publications **25**, 5780–5786.

39 Foguel, D. and Silva, J. L. (1994) Cold denaturation of a repressor-operator complex: the role of entropy in protein-DNA recognition. Proc. Natl. Acad. Sci., National Academy of Sciences **91**, 8244–8247.

40 Sampson, D. A., Wang, M. and Matunis, M. J. (2001) The small ubiquitin-like modifier-1 (SUMO-1) consensus sequence mediates Ubc9 binding and is essential for SUMO-1 modification. J. Biol. Chem., ASBMB **276**, 21664–21669.

41 Bernier-Villamor, V., Sampson, D. A., Matunis, M. J. and Lima, C. D. (2002) Structural basis for E2-mediated SUMO conjugation revealed by a complex between ubiquitin-conjugating enzyme Ubc9 and RanGAP1. Cell, Elsevier **108**, 345–356.

42 Moutty, M. C., Sakin, V. and Melchior, F. (2011) Importin α/β mediates nuclear import of individual SUMO E1 subunits and of the holo-enzyme. Mol. Biol. Cell, Am Soc Cell Biol **22**, 652–660.

43 Olsen, S. K., Capili, A. D., Lu, X., Tan, D. S. and Lima, C. D. (2010) Active site remodelling accompanies thioester bond formation in the SUMO E1. Nature, Nature Publishing Group **463**, 906–912.

44 Giraud, M., Desterro, J. M. P. and Naismith, J. H. (1998) Structure of ubiquitin-conjugating enzyme 9 displays significant differences with other ubiquitin-conjugating enzymes which may reflect its specificity for sumo rather than ubiquitin. Acta Crystallogr. Sect. D Biol. Crystallogr., International Union of Crystallography **54**, 891–898.

45 Bencsath, K. P., Podgorski, M. S., Pagala, V. R., Slaughter, C. A. and Schulman, B. A. (2002) Identification of a multifunctional binding site on Ubc9p required for Smt3p conjugation. J. Biol. Chem., ASBMB **277**, 47938–47945.

Table 1. Summary of crystallographic analysis

Data collection		
	AtSCE1	**AtSCE1 - AtUFD**
Beamline	ALBA-XALOC	ALBA-XALOC
Space group	$P2_12_12_1$	$P2_1$
Wave length (Å)	0.9793	0.9792
Resolution (Å)	50.38-1.201 (1.205-1.201)	58.82-1.792 (1.798-1.792)
a, b, c (Å)	32.90, 50.38, 93.78	36.16, 58.82, 70.23
α, β, γ (°)	α = β = γ = 90	α = γ = 90, β = 92.05
Unique reflections	49524	26999
Data redundancy	6.0 (6.2)	3.4 (3.3)
R_{merge}	0.14 (1.45)	0.094 (0.97)
CC(1/2)	0.996 (0.642)	0.992 (0.581)
I/σ	9.5 (2.2)	8.5 (1.7)
Completeness (%)	99.9 (93.6)	99.9 (93.6)
Refinement		
Resolution (Å)	44.38 – 1.20	45.08 – 1.80
Non-anomalous reflections	49227	26964
R_{work}/R_{free}	0.19/0.21	0.17/0.22
Number of all atoms	1310	2212
Number of waters	188	68
RMSD bond (Å)/Angle (°)	0.014/1.50	0.017/1.62
Ramachandran plot		
Favored (%)	95.52	97.30
Allowed (%)	3.73	2.70
Disallowed (%)	0.75	0

* Highest resolution shell is shown in parenthesis.

Figures Legends

Fig. 1. SUMO conjugation assays exchanging SUMOs between human and Arabidopsis systems. *A,* SDS-PAGE analysis of the conjugation assays using human SUMO1 & 2 with E1 and E2 enzymes from human and Arabidopsis at pH 8.5. *B*, SDS-PAGE analysis of the conjugation assays using Arabidopsis SUMO1 & 2 with E1 and E2 enzymes from human and Arabidopsis. *C.* Analysis of the SUMO-E1 and SUMO-E2 thioester formation (indicated with an ~ hyphen). Gels were run in the absence of b-mercaptoethanol. *D*, End-point reaction after 120 minutes of the heterologous conjugation assays combining SUMO1 and SUMO2 from human and Arabidopsis, respectively, with E1 and E2 enzymes from human and Arabidopsis.

Fig 2. Purification of the complex between AtSCE1 and AtUFDC or AtUFD. *Above*, elution profile of the gel filtration purification (SUPERDEX 75 column) after mixing equimolar concentrations of AtSCE1 with either AtUFD (*A*), or AtUFDC (*B*) in a buffer containing 25mM HEPES 7.0, 100mM NaCl. Dotted lines indicated the elution volumes of the individual components. *Below*, SDS-PAGE analysis of the fractions of the elution peak is shown below.

Fig 3. Crystal structure of the AtSCE1 and AtUFD-SCE1 complex. *A*, Cartoon representation of the structure of AtSCE1. *B*, Structural alignment of the isolated (yellow) and complexed (green) SCE1. *C*, Cartoon representation of the structure of AtUFD-SCE1 complex. Interface elements α1 helix and the β1-β2 loop of SCE1 are indicated. *D*, Structural alignment of the isolated AtSCE1 and human Ubc9 (PDB code 1A3S). Backbone differences are depicted. *E*, Superimposition of the AtUFD-SCE1 complex on the human hUFD-Ubc9 complex (PDB code 5FQ2) by alignment of the SCE1 and human Ubc9. *F*, Superimposition of the AtUFD-SCE1 complex on the human hUFD-Ubc9 complex (PDB code 5FQ2) by alignment of the UFD domains. *G*, Structure alignment of the isolated AtSCE1 and yeast Ubc9 (PDB code 2GJD). *H*, Superimposition of the AtUFD-SCE1 complex on the yeast yUFD-Ubc9 complex (PDB code 3ONG) by alignment of the SCE1 and yUbc9. *I*, Superimposition of the AtUFD-SCE1 complex on the yeast yUFD-Ubc9 complex (PDB code 3ONG) by alignment of the UFD domains.

Fig 4. Structural and sequential comparison of Arabidopsis SCE1, human and yeast Ubc9. *A*, Cartoon and transparent electrostatic surface representation of AtSCE1, human Ubc9 and yeast Ubc9. Contact residues are labeled and shown in stick representation. *B*, Structural sequence alignment of Arabidopsis AtSCE1, human and yeast Ubc9. AtSCE1 domain secondary structure is shown on top. Red triangles indicate AtSCE1 contacts with AtUFD domain.

Fig 5. Structural details and the comparison of the UFD domains. *A*, Cartoon representation of the structural overlapping of Arabidopsis AtUFD (blue) and human hUFD (red). *B*, stereo cartoon representation of the contacts between AtSCE1 (yellow thin ribbon) and AtUFD E1 domain (blue cartoon). Side-chain contact residues are labeled and shown in stick representation. *C*, Structural sequence alignment of the UFD domains of Arabidopsis (AtUFD), human (HsUFD) and yeast (ScUFD). AtUFD domain secondary structure is shown on top. Red triangles indicate AtUFD contacts with SCE1. Dotted red rectangle indicates the predicted LHEB2 region. *D*, Schematic representation of SUMO UFD domain contacts with the E2 enzymes from Arabidopsis, human (PDB code 5FQ2), and yeast (PDB code 3ONG).

Fig 6. Activity, pull-down, and protein unfolding assays of AtSCE1 mutants. *A*, SDS-PAGE of time-course SUMO conjugation assays of AtSCE1 mutants compared to the wild type AtSCE1 at pH 7.5. *B*, SDS-PAGE of the pull-down assays of wild type AtSCE1 (WT) and indicated AtSCE1 mutants. Panel below displays loading control for AtSCE1 wild type and mutants. *C*, Comparison of the temperature and urea induced protein unfolding curves of wild type AtSCE1 and the AtSCE1 R7L/G8S/K28V/V37M mutant.

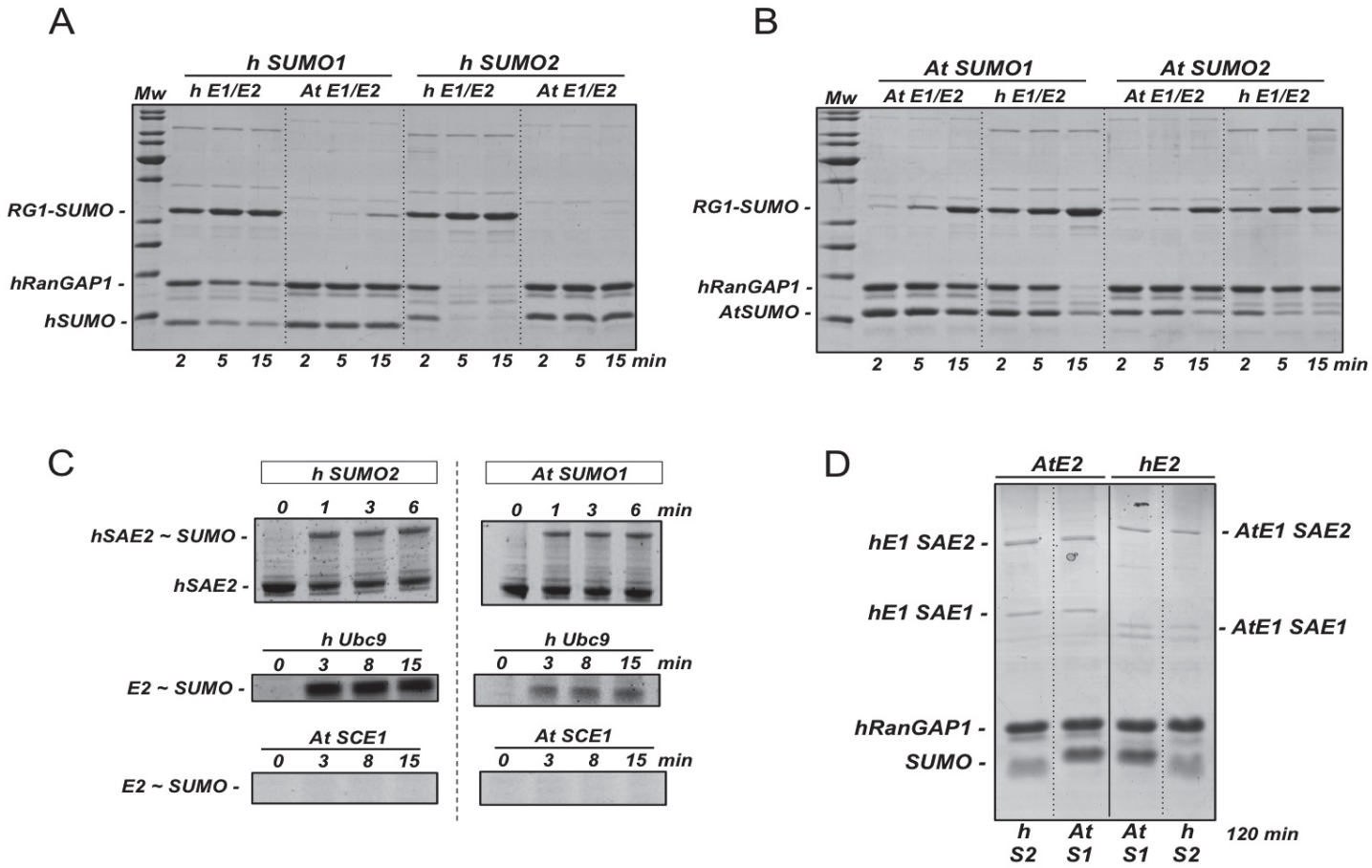
A
h SUMO1
h SUMO2
Mw
h E1/E2
At E1/E2
h E1/E2
At E1/E2
RG1-SUMO -
hRanGAP1 -
hSUMO -
2 5 15 2 5 15 2 5 15 2 5 15 min
B
At SUMO1
At SUMO2
Mw
At E1/E2
h E1/E2
At E1/E2
h E1/E2
RG1-SUMO -
hRanGAP1 -
AtSUMO -
2 5 15 2 5 15 2 5 15 2 5 15 min
C
h SUMO2
At SUMO1
0 1 3 6 min
hSAE2 ~ SUMO -
hSAE2 -
h Ubc9
0 3 8 15 min
E2 ~ SUMO -
At SCE1
0 3 8 15 min
E2 ~ SUMO -
D
AtE2
hE2
hE1 SAE2 -
hE1 SAE1 -
- AtE1 SAE2
- AtE1 SAE1
hRanGAP1 -
SUMO -
h S2
At S1
At S1
h S2
120 min

Figure 1

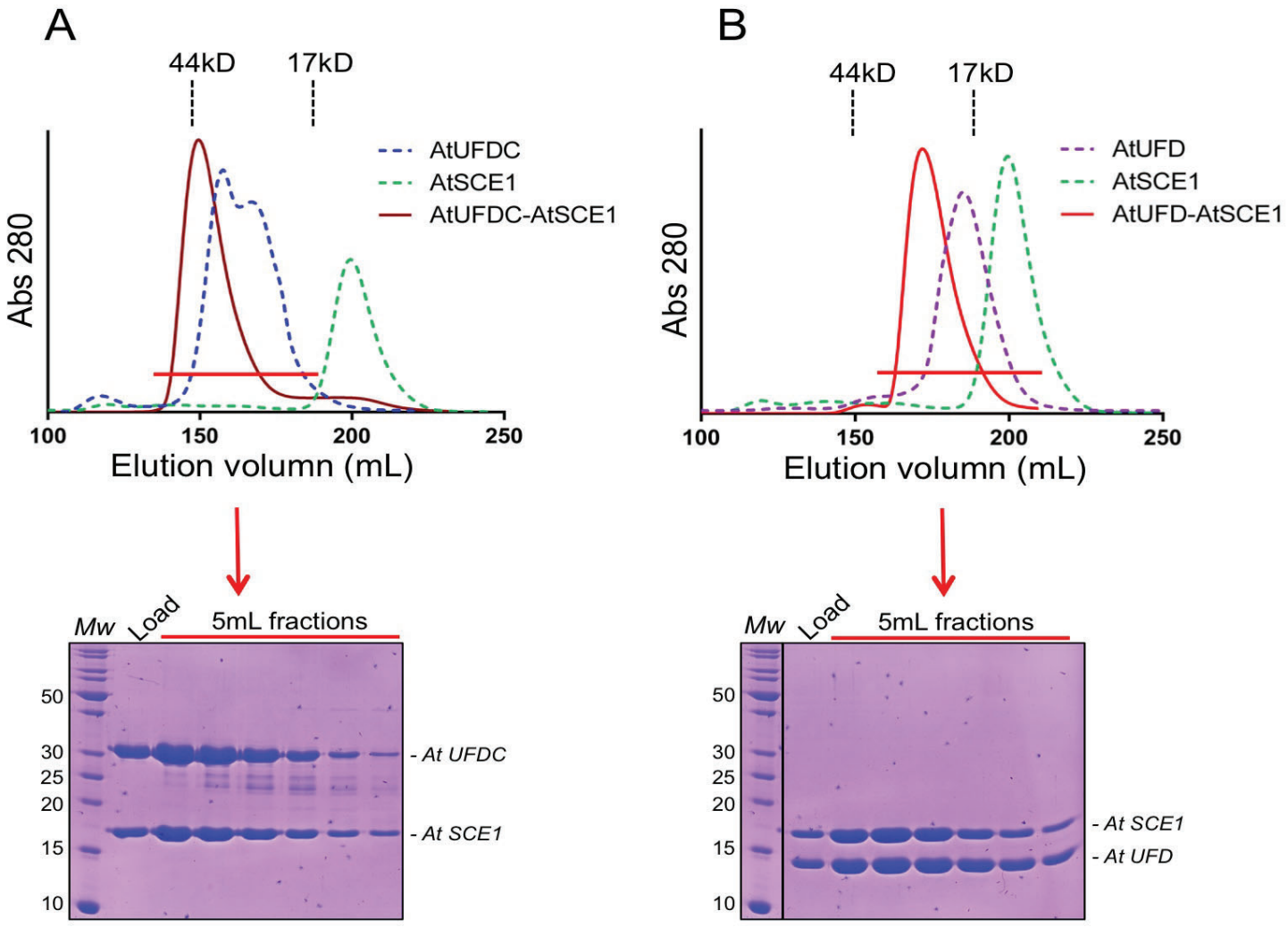
A
44kD
17kD
AtUFDC
AtSCE1
AtUFDC-AtSCE1
Abs 280
100
150
200
250
Elution volumn (mL)
Mw
Load
5mL fractions
50
30
25
20
15
10
- At UFDC
- At SCE1
B
44kD
17kD
AtUFD
AtSCE1
AtUFD-AtSCE1
Abs 280
100
150
200
250
Elution volumn (mL)
Mw
Load
5mL fractions
50
30
25
20
15
10
- At SCE1
- At UFD

Figure 2

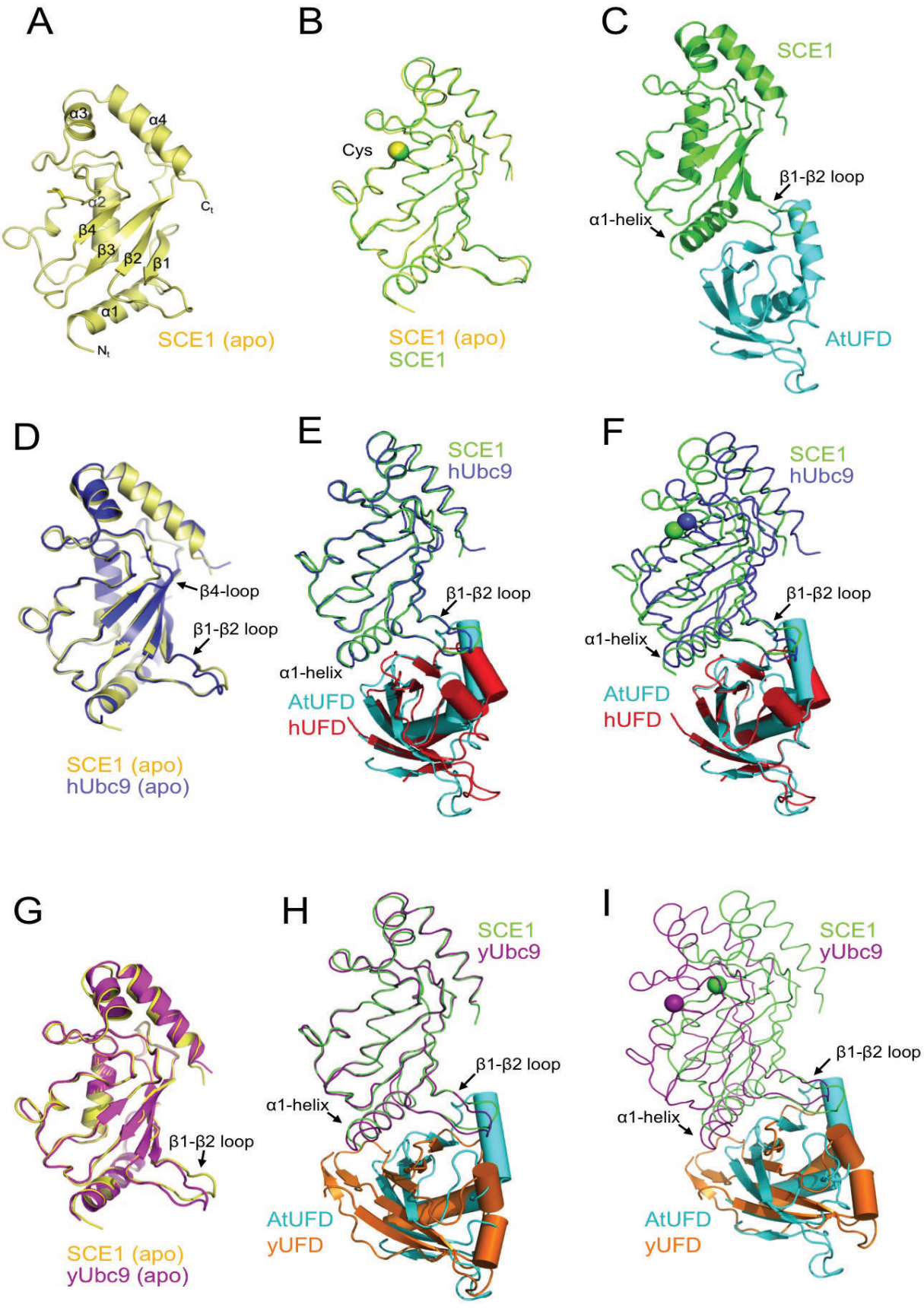
A
α3
α4
α2
β4
β3
β2
β1
α1
Ct
Nt
SCE1 (apo)
B
Cys
SCE1 (apo)
SCE1
C
SCE1
β1-β2 loop
α1-helix
AtUFD
D
β4-loop
β1-β2 loop
SCE1 (apo)
hUbc9 (apo)
E
SCE1
hUbc9
β1-β2 loop
α1-helix
AtUFD
hUFD
F
SCE1
hUbc9
β1-β2 loop
α1-helix
AtUFD
hUFD
G
β1-β2 loop
SCE1 (apo)
yUbc9 (apo)
H
SCE1
yUbc9
β1-β2 loop
α1-helix
AtUFD
yUFD
I
SCE1
yUbc9
β1-β2 loop
α1-helix
AtUFD
yUFD

Figure 3

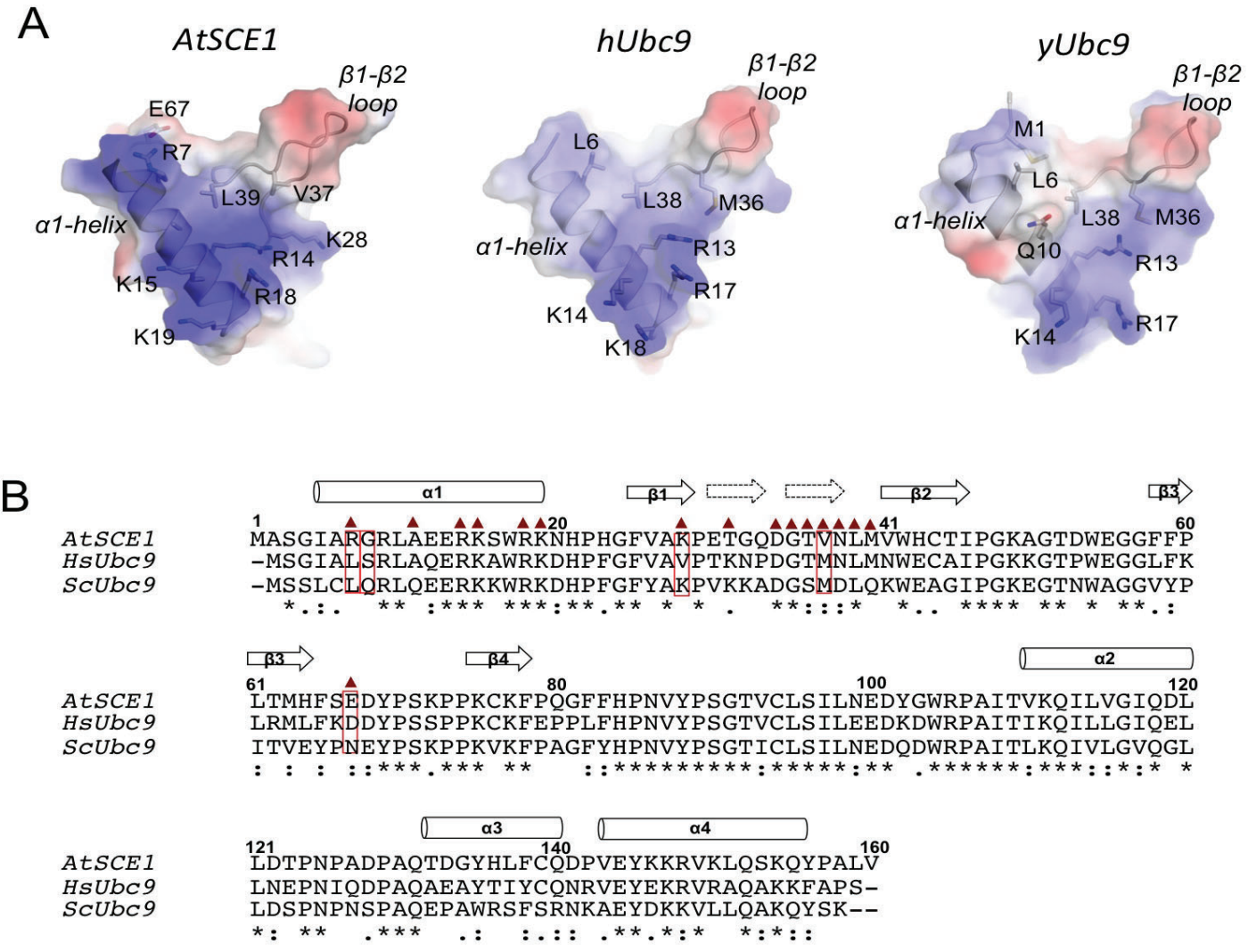
A
AtSCE1
β1-β2 loop
E67
R7
L39
V37
α1-helix
K28
R14
K15
R18
K19
hUbc9
β1-β2 loop
L6
L38
M36
α1-helix
R13
R17
K14
K18
yUbc9
β1-β2 loop
M1
L6
α1-helix
L38
M36
Q10
R13
R17
K14
B
α1
β1
β2
β3
AtSCE1 MASGIARGRLAEERKSWRKNHPHGFVAKPETGQDGTVNLMVWHCTIPGKAGTDWEGGFFP
HsUbc9 -MSGIALSRLAQERKAWRKDHPFGFVAVPTKNPDGTMNLMNWECAIPGKKGTPWEGGLFK
ScUbc9 -MSSLCLQRLQEERKKWRKDHPFGFYAKPVKKADGSMDLQKWEAGIPGKEGTNWAGGVYP
β3
β4
α2
AtSCE1 LTMHFSEDYPSKPPKCKFPQGFFHPNVYPSGTVCLSILNEDYGWRPAITVKQILVGIQDL
HsUbc9 LRMLFKDDYPSSPPKCKFEPPLFHPNVYPSGTVCLSILEEDKDWRPAITIKQILLGIQEL
ScUbc9 ITVEYPNEYPSKPPKVKFPAGFYHPNVYPSGTICLSILNEDQDWRPAITLKQIVLGVQGL
α3
α4
AtSCE1 LDTPNPADPAQTDGYHLFCQDPVEYKKRVKLQSKQYPALV
HsUbc9 LNEPNIQDPAQAEAYTIYCQNRVEYEKRVRAQAKKFAPS-
ScUbc9 LDSPNPNSPAQEPAWRSFSRNKAEYDKKVLLQAKQYSK--

Figure 4

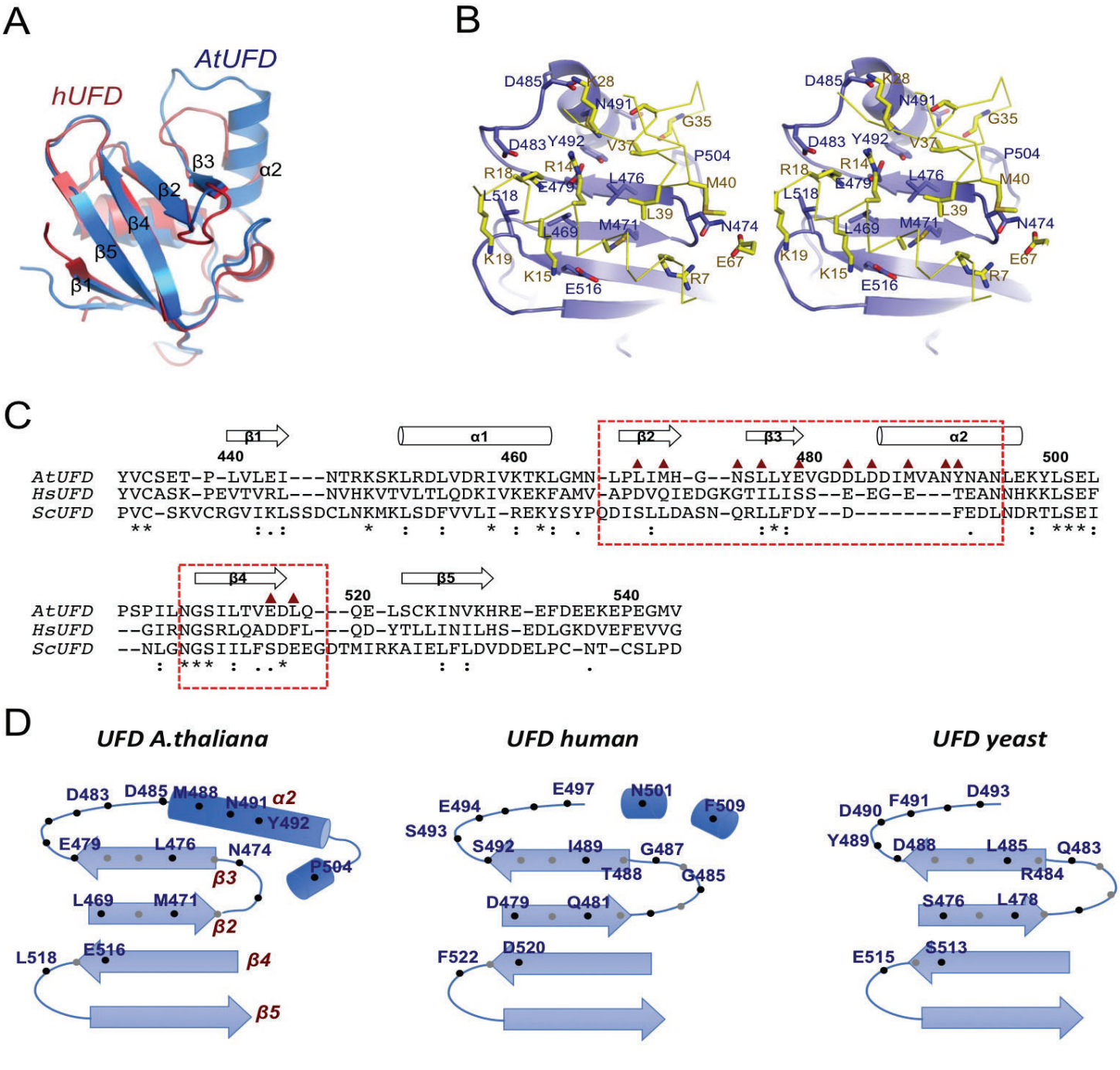
A
AtUFD
hUFD
β3
α2
β2
β4
β5
β1
B
D485
K28
N491
G35
D483
Y492
V37
P504
R14
R18
E479
L476
M40
L518
L39
L469
M471
N474
K19
E67
K15
R7
E516
C
β1
α1
β2
β3
α2
440
460
480
500
AtUFD YVCSET-P-LVLEI---NTRKSKLRDLVDRIVKTKLGMN-LPLIMH-G--NSLLYEVGDDLDDIMVANYNANLEKYLSEL
HsUFD YVCASK-PEVTVRL---NVHKVTVLTLQDKIVKEKFAMV-APDVQIEDGKGTILISS--E-EG-E---TEANNHKKLSEF
ScUFD PVC-SKVCRGVIKLSSDCLNKMKLSDFVVLI-REKYSYPQDISLLDASN-QRLLFDY--D--------FEDLNDRTLSEI
β4
β5
520
540
AtUFD PSPILNGSILTVEDLQ---QE-LSCKINVKHRE-EFDEEKEPEGMV
HsUFD --GIRNGSRLQADDFL---QD-YTLLINILHS-EDLGKDVEFEVVG
ScUFD --NLGNGSIILFSDEEGDTMIRKAIELFLDVDDELPC-NT-CSLPD
D
UFD A.thaliana
UFD human
UFD yeast
D483
D485
M488
N491
α2
Y492
E479
L476
N474
β3
P504
L469
M471
β2
L518
E516
β4
β5
E497
N501
E494
F509
S493
S492
I489
G487
T488
G485
D479
Q481
F522
D520
D490
F491
D493
Y489
D488
L485
Q483
R484
S476
L478
E515
S513

Figure 5

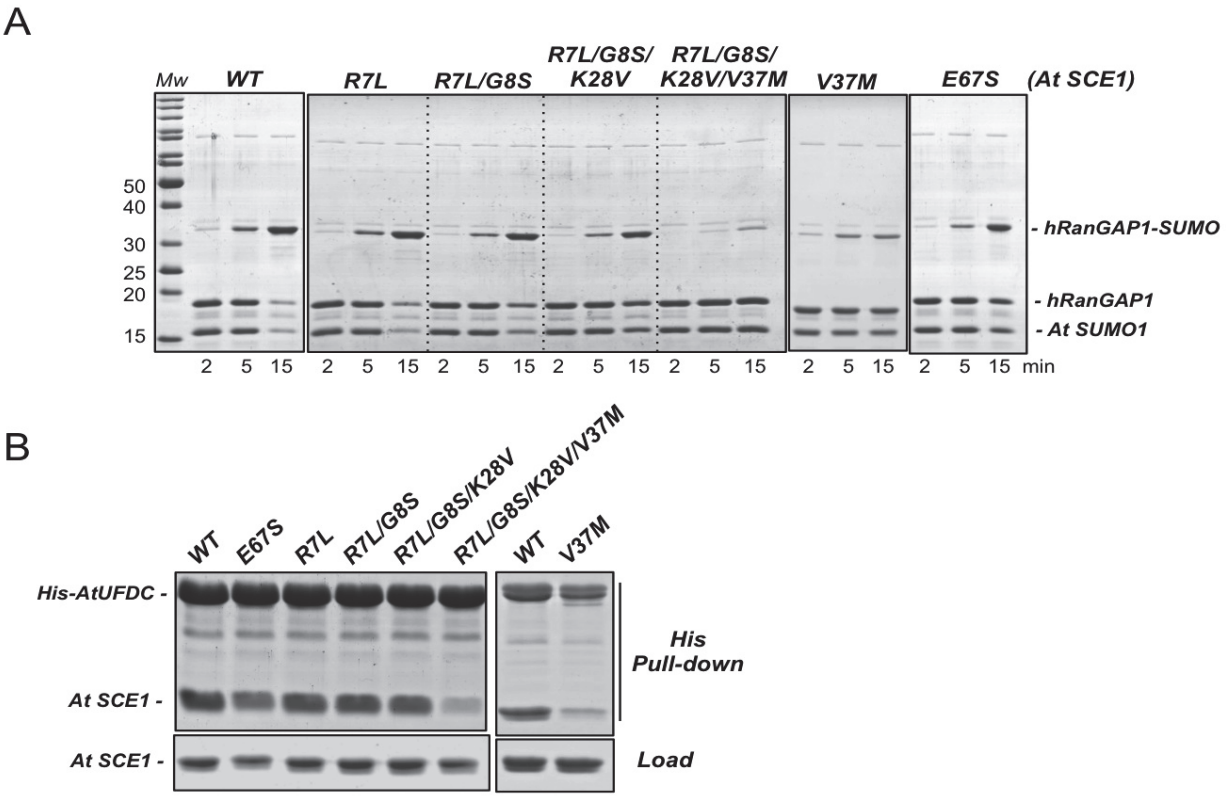
A
Mw
WT
R7L
R7L/G8S
R7L/G8S/ K28V
R7L/G8S/ K28V/V37M
V37M
E67S
(At SCE1)
50
40
30
25
20
15
- hRanGAP1-SUMO
- hRanGAP1
- At SUMO1
2 5 15 2 5 15 2 5 15 2 5 15 2 5 15 2 5 15 2 5 15 min
B
WT
E67S
R7L
R7L/G8S
R7L/G8S/K28V
R7L/G8S/K28V/V37M
WT
V37M
His-AtUFDC -
At SCE1 -
His Pull-down
At SCE1 -
Load
C
Fraction unfolded
1.0
0.5
0.0
AtSCE1
R7L/G8S/K28V/V37M
30 40 50 60 70 80
Temperature (°C)
Fraction unfolded
1.0
0.5
0.0
AtSCE1
R7L/G8S/K28V/V37M
0 2 4 6 8
Urea (M)

Figure 6